IEEE Access
Multidisciplinary ⋮ Rapid Review ⋮ Open Access Journal

Received February 7, 2022, accepted February 23, 2022, date of publication February 25, 2022, date of current version March 4, 2022.

Digital Object Identifier 10.1109/ACCESS.2022.3154790

WiSig: A Large-Scale WiFi Signal Dataset for Receiver and Channel Agnostic RF Fingerprinting

SAMER HANNA, (Graduate Student Member, IEEE),
SAMURDHI KARUNARATNE, (Graduate Student Member, IEEE),
AND DANIJELA CABRIC, (Fellow, IEEE)
Electrical and Computer Engineering Department, University of California, Los Angeles, CA 90095, USA

Corresponding author: Samer Hanna (samerhanna@ucla.edu)

This work was supported in part by the CONIX Research Center, one of six centers in JUMP, a Semiconductor Research Corporation (SRC) Program by DARPA.

ABSTRACT RF fingerprinting leverages circuit-level variability of transmitters to identify them using signals they send. Signals used for identification are impacted by a wireless channel and receiver circuitry, creating additional impairments that can confuse transmitter identification. Eliminating these impairments or just evaluating them, requires data captured over a prolonged period of time, using many spatially separated transmitters and receivers. In this paper, we present WiSig; a large-scale WiFi dataset containing 10 million packets captured from 174 off-the-shelf WiFi transmitters and 41 USRP receivers over 4 captures spanning a month. WiSig is publicly available, not just as raw captures, but as conveniently pre-processed subsets of limited size, along with the scripts and examples. A preliminary evaluation performed using WiSig shows that changing receivers, or using signals captured on a different day can significantly degrade a trained classifier's performance. While capturing data over more days or more receivers limits the degradation, it is not always feasible, and novel data-driven approaches are needed. WiSig provides the data to develop and evaluate these approaches towards channel and receiver agnostic transmitter fingerprinting.

INDEX TERMS RF fingerprinting, transmitter identification, WiFi dataset.

I. INTRODUCTION

Each transmitter has a unique radio frequency (RF) fingerprint that is caused by the manufacturing variability of its circuit design and components. This variability makes two transmitters, from the same make and model, sending the same waveforms, have slight differences in their signals. Transmitter (Tx) RF fingerprinting leverages these subtle unintentional differences in the signals to identify transmitters. Tx fingerprinting has the potential of improving the security of wireless networks by verifying the identities of transmitters without imposing any transmitter-side overheads.

Since RF fingerprints are not designed but result from manufacturing variability, they need to be extracted using data-driven approaches from the captured signals. However, captured signals contain confounding factors besides the transmitter fingerprint: a channel fingerprint is added as the signals propagate through a wireless channel. Also, receivers suffer from manufacturing variability same as transmitters, hence, the receiver RF fingerprint is also embedded in the signal. Data-driven approaches like deep learning are easily confounded by both the channel and receivers. In [1], it was shown that evaluating the same transmitter in a different channel can cause the accuracy of a classifier to drop from 85% to 9%. Similar trends were reported in [2] for the impact of receivers. Practical deployments of RF fingerprinting systems can involve hundreds of transmitters and need to work over prolonged periods of times where the channel varies. Additionally, aside from micro-scale deployments, many receivers need to participate in the fingerprinting system, and training a classifier per receiver might not be practical. These facts drive the need for a channel and receiver agnostic transmitter RF fingerprinting system. The first step in building such an RF fingerprinting system is having suitable data that enables isolating and evaluating both the channel and receiver impacts.

Many existing works on RF fingerprinting have relied on data collected using custom testbeds. In the IoT space, several works have used LoRa and ZigBee testbeds. In [3], several signal representations were considered using signals

The associate editor coordinating the review of this manuscript and approving it for publication was Moussa Ayyash.

from 25 LoRa devices captured over several days. To consider the impact of channel, indoor and outdoor captures were performed using 100 LoRa transmitters in [4]. In [5], the problem of identifying unseen devices was approached using 60 LoRa devices. Using a capture of 54 ZigBee radios, the multi-sampling convolutional neural network was proposed for RF fingerprinting [6]. These previous works have only considered a single USRP receiver.

The impact of changing receivers on transmitter fingerprinting was studied in [2], where signals from 25 ZigBee devices were captured using 10 receivers over a single capture. To the best of the authors' knowledge, these datasets are not publicly accessible. In [7], RF fingerprinting was evaluated under several experimental scenarios using 25 LoRa devices and 2 receivers with the dataset publicly available. Other works have used USRPs to send signals following different protocols: in [1], 20 USRPs sending WiFi signals were used to study the impact of the channel. Four USRPs sending multiple signals (5G New Radio, LTE, WiFi) were fingerprinted in [8]. Although the datasets used in [1], [8] are publicly accessible, they only considered one receiver. Besides, USRPs have fundamentally different hardware than commercial radios and thus their transmitter fingerprints do not necessarily represent commonly used radios. All the previous datasets included at most 100 transmitters. The largest RF fingerprinting dataset reported in the literature is the DARPA RFMLS dataset [9]; it consists of signals from 5117 WiFi Tx captured using a spectrum analyzer and 5000 ADS-B devices [10]. This dataset was used by many works [1], [10], [11]; however, it is not publicly accessible. In our previous work [12], we considered a WiFi dataset using 163 WiFi transmitters captured in the Orbit testbed [13], but it only considered one receiver. The previously discussed datasets are summarized in Table 1.

In this work, we present the WiSig dataset, including 10 million WiFi packets transmitted by 174 off-the-shelf WiFi transmitters and captured by 41 USRP receivers in four different captures performed over a month. To the best of the authors' knowledge, this dataset is the largest publicly available dataset and the first to include such a large number of both transmitters and receivers. Our focus was on making the dataset widely accessible and easy to use. Instead of only making the 1.4 TB raw dataset (*Raw WiSig*) available, we also provide a 76.9 GB processed dataset (*Full WiSig*) containing directly usable WiFi preambles.[1] Furthermore, we provide conveniently pre-packaged subsets only a few GB in size. Using these subsets, in this paper, we showcase example uses of WiSig and identify some open problems in RF fingerprinting. The scripts to generate the results in this paper are publicly available. We also provide the scripts to process the raw signals, create custom subsets, along with the commands to replicate the capture in a private testbed. Our main contributions can be summarized as follows

TABLE 1. Summary of related datasets.

Ref	Transmitters	Receiver(s)	Many Days	Public
[3]	25 LoRa	1 USRP	Yes	No
[4]	100 LoRa	1 USRP	Yes	No
[5]	60 LoRa	1 USRP	No	No
[6]	54 ZigBee	1 USRP	No	No
[12]	163 WiFi	1 USRP	Yes	No
[7]	25 LoRa	2 USRP	Yes	Yes
[2]	25 ZigBee	10 USRP, Spectrum analyzer	No	No
[1]	20 USRP (WiFi signal)	1 USRP	Yes	Yes
[8]	4 USRP (signals: 5G New Radio, LTE, WiFi)	10 USRP, Spectrum analyzer	No	Yes
[9]	5117 WiFi , 5000 ADS-B	RF Spectrum analyzer	Yes	No

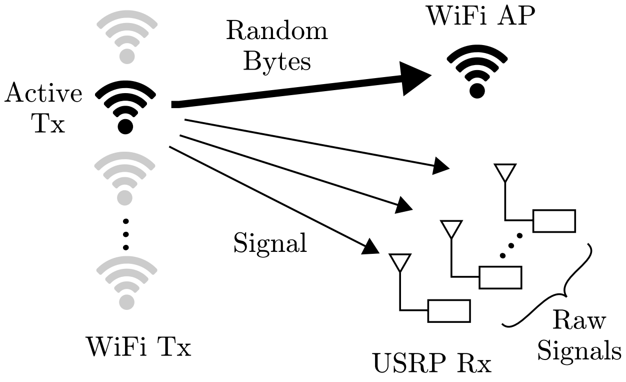

FIGURE 1. The capture setup. The active Tx sends random bytes using UDP to a WiFi access point. The USRP Rx capture the signals over the same band.

- We provide a large-scale WiFi dataset captured by 41 USRP receivers from 174 WiFi transmitters over four different captures performed within a month.
- We showcase how the dataset can be used to study the performance of RF fingerprinting as we change the number of transmitters, receivers, days, and signals.
- We identify some open problems in RF fingerprinting that can be addressed using this dataset.

The rest of the paper is organized as follows: in Section II, we provide an overview of the dataset creation. The data capture, signal extraction, and dataset assembly are described in Sections III, IV, and V respectively. Use cases of the dataset along with open problems are provided in Section VI. Section VII concludes the paper.

II. DATASET OVERVIEW

The dataset consists of USRP captures of signals sent from a WiFi node to a WiFi access point (AP); the WiFi nodes are the transmitters to fingerprint, the USRPs are the receivers, and the WiFi AP is needed to establish the WiFi link. The capture from one WiFi transmitter works as follows; a transmitter sends data to the AP while all the USRP receivers continuously capture the raw IQ samples as illustrated in Fig. 1.

[1] https://cores.ee.ucla.edu/downloads/datasets/wisig/

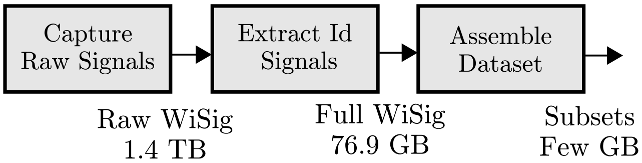

FIGURE 2. The process for creating the dataset. Raw signals are captured, then the identification signals are extracted, and finally, the dataset is assembled. The size of the data decreases after each stage.

In a single day, captures were performed from all contributing transmitters, one at a time, in a fully automated manner. The raw IQ samples for the entire duration of the transmission are stored, including idle time. Four single-day captures are performed over a month to create the Raw WiSig dataset. The Raw WiSig dataset has a large size of 1.4 TB and needs to be processed before usage.

We performed the processing to create the *Identification (Id) signals* that can be easily used as input to a classifier. As processing, we detected the packets and isolated them. After packet detection, two types of identification signals are created; the first one uses the first 256 IQ samples from each packet without further processing. In the second one, the packet is equalized, using the WiFi preambles, before extracting the first 256 IQ samples. All Id signals (non-equalized and equalized) constitute the Full WiSig dataset. The Full WiSig dataset size is 76.9 GB, which is still considerably large. Due to many sources of randomness in the capture, Full WiSig is not balanced; that is, not all transmitter-receiver pairs have the same number of signals. Additionally, a typical user will probably only use a subset of the signals and might not need the entire Full WiSig.

For convenience, we assembled four subsets of the Full WiSig dataset to cater to the needs of different dataset users. These subsets are called ManyTx, ManyRx, ManySig, SingleDay. ManyTx, ManyRx, ManySig provide a large number of Tx, Rx, or signals, respectively, covering all four days. SingleDay provides an appreciable number of Tx, Rx, and signals in just one day. These subsets are pre-packaged and only require a download of a few gigabytes. An overview of these steps is highlighted in Fig. 2. The scripts to process the dataset from one stage to the next one are provided so that the user can modify each processing step easily, if needed. We also provide scripts that enable the users to repeat the capture setup using their own hardware. In the following sections, we describe each stage in detail.

III. CAPTURING RAW SIGNALS

The dataset was captured in the Orbit testbed [13]. The Orbit testbed consists of a 20 × 20 grid of nodes with a separation of 3 feet (about 1m). Each node is a roof-mounted computer equipped with at least one WiFi radio; some nodes are equipped with USRPs. An image of the Orbit grid is shown in Fig. 3. In addition to the grid, some USRPs are placed in the same room as part of two massive MIMO racks. The locations of the WiFi transmitters and the USRP Rx are shown in Fig. 4. The WiFi 802.11 a/g modules used are Atheros 5212, 9220, 9280, and 9580; the USRPs are B210, X310, and N210. Note that the USRPs with x-position larger than 20 in Fig. 4b are part of the massive MIMO racks. The captures were performed on four days: the 1st, 8th, 15th, and 23rd of March 2021.

FIGURE 3. Orbit nodes are arranged as a grid. Each node is a roof-mounted PC with at least one WiFi module. Some nodes are equipped with USRPs.

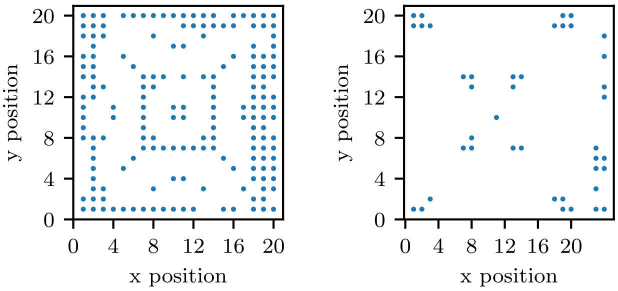

(a) Transmitters

(b) Receivers

FIGURE 4. Positions of Tx and Rx in the Orbit grid. Rx with x position greater than 20 are part of the massive MIMO racks.

We start by describing the WiFi transmitters (Tx), AP, and USRP receivers configurations. The WiFi 802.11 a/g Tx and AP were configured to operate over WiFi channel 11 having a center frequency of 2462MHz and a bandwidth of 20MHz. This channel was chosen because no non-participating WiFi APs were detected on this channel. However, the Orbit grid is not RF isolated and external interference is possible. To avoid any data clues about the identity of the WiFi transmitter, all transmitters were configured to have the same spoofed MAC address and the same IP address when connected. The WiFi payload consisted of UDP packets carrying a stream of random bytes. The USRP receivers captured IQ samples at a rate of 25 Msps with a center frequency of 2462MHz for a duration of 0.512s. Due to the mostly line-of-sight channel, the signals are at high SNR (>10dB). Note that the number of WiFi packets transmitted within the capture duration is determined by the WiFi MAC protocol and hence it varies per capture. Also note that all USRP receivers operated independently without any time or frequency synchronization. Due to the delays in processing the commands, there is no guarantee that the captures are aligned in time; that is some receivers might start the capture earlier or later than others.

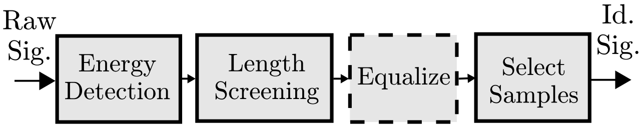

FIGURE 5. The processing flow for extracting the identification signals from the raw signals. Two types of Id signals are created, one with and the other without equalization.

The number of WiFi transmitters that participated in all the captures was 174 and the number of USRP receivers was 41. However, not all transmitters or receivers participated in all days of the data capture for several reasons; (1) On some days, some transmitters or receivers were not accessible in the Orbit testbed (2) A transmitter or receiver can run into hardware or software problems on one or multiple occasions. Due to the large scale of the experiment, it was not feasible to stop the experiment and manually debug each transmitter or receiver. As a consequence, there is no data for some transmitter-receiver pairs in the raw dataset on some days. Note that if the transmitter did not operate, the USRPs would still capture a signal and this case needs to be handled in processing.

IV. EXTRACTING IDENTIFICATION SIGNALS

To obtain the Id Signals (both non-equalized and equalized), we start by detecting the packets and eliminating irrelevant signals. Then we perform equalization for one version of the Id signal, then we choose the samples to be used as illustrated in Fig. 5.

A. ENERGY DETECTION AND SCREENING

In this stage, our objective is to identify the IQ samples corresponding to transmissions from the WiFi nodes and exclude other signals in the spectrum like the ACK response from the WiFi AP and non-WiFi signals that might exist. We start by detecting signals and then excluding the ACKs. The signal detection was performed by comparing the signal magnitude in a window consisting of N_w IQ samples to a fixed threshold L_w. As for identifying the packets from the ACK, we relied on signal durations and the fact that each WiFi packet is much longer than the fixed duration ACK signal that follows it. We considered a valid packet as a signal of length larger than N_{pkt} followed immediately by a signal shorter than N_{ack}. Both the packet detection and isolation were performed without using the known WiFi preambles. While this is not ideal from a detection perspective, it is simple to implement and emulates the processing for protocol agnostic transmitter fingerprinting, even though we do not consider it in this work. We used $N_w = 100$, $L_w = 0.005$, $N_{pkt} = 1000$, and $N_{ack} = 2000$ in our detection script. These values were obtained empirically by visually inspecting the captured IQ samples. After isolating the packets, for some transmitters only a few packets were detected, which might indicate that the transmitter did not turn on properly and these packets were erroneously detected. So, transmitters with exceptionally few captured packets (specifically, less than 10) were eliminated.

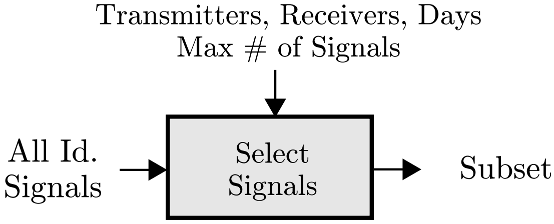

FIGURE 6. The dataset assembly flow. A subset is created from all the identification signals by specifying the list of Tx, Rx, days, and the maximum number of signals to retain.

B. EQUALIZATION AND SELECTING SAMPLES

Using the isolated packets, two datasets were built; the first one contains part of the unprocessed preambles, the second includes equalization. For the first dataset, the first 256 IQ samples of each packet were included along with the transmitter, receiver, and day labels. In the second dataset, the preambles were equalized. To equalize the packets, we used the WiFi packet structure, which starts with two preambles: the L-STF and L-LTF preambles [14]. First, we resampled the packet to change its sampling rate from 25 Msps to 20 Msps because it is the nominal sampling rate for WiFi. Then autocorrelation is applied on the L-STF preamble to accurately detect the packet start. If the preamble is detected the frequency offset is estimated and corrected, else the packet is discarded. The L-STF preamble misdetection can be due to the misidentification of the start of the signal using energy detection or caused by a mistakenly captured a non-WiFi signal. For the detected packets, the channel is then estimated using the L-LTF and the signal is equalized using MMSE. The signal processing for detection and channel estimation was applied using MATLAB R2019b WLAN toolbox with the default parameters. Afterwards, the frequency offset is reapplied to the signal to be used for fingerprinting. The signal is then resampled back to 25 Msps and the first 256 samples were included in the dataset along with the transmitter and receiver labels. After equalization, the transmitters with few packets were eliminated again. The scripts to perform these steps are provided with the downloads.

V. DATASET ASSEMBLY

After capturing and processing the data, a WiSig user would typically choose a subset of the dataset that meets the user's requirements. This subset is chosen by providing a list of Tx, Rx, days, and the maximum number of signals as illustrated in Fig. 6. We start by analyzing the number of signals and present a method to select a subset of the dataset. We also discuss the prepackaged subsets provided for the convenience of WiSig users.

A. DATASET ANALYSIS

After processing the dataset, we analyze the number of collected Id signals $C(d, t, r)$ on day d, from transmitter t, and receiver r. The total number of Id signals, that is $\sum_{d,t,r} C(d, t, r)$, is equal to 9.97 million using 174 Tx, 41 Rx, over 4 days. As discussed earlier, some transmitters and receivers failed on some days. Also, the number of WiFi packets transmitted varied due to the WiFi MAC rate control. Additionally, due to the lack of synchronization along with detection errors, the number of Id signals varied among Rx. All these factors make the dataset imbalanced as the number of Id signals C depends on d, t, as well as r. To visualize C, in Fig. 7, we plot $C(d, t, r)$ for the first day $d = 0$. The x and y axis are identifiers for the particular Tx and Rx respectively, and the logarithmic colormap indicates the count of Id signals. To visualize all the counts, in Fig. 8, we plot the histogram of C below 2000 for all d, t, and r. From this figure, we see that the majority of Tx-Rx-day counts $C(d, t, r)$, is below 400. A smaller number of Tx-Rx-day counts (C) exceeded 1000, and a few even exceeded 2000 but were not included in the histogram for clarity. Note that because the L-LTF preamble detection for some signals, the number of collected signals for the equalized signals $C_{\text{eq}}(d, t, r)$ might be slightly smaller than the non-equalized dataset, that is $C_{\text{eq}}(d, t, r) \leq C(d, t, r)$.

The large imbalance of $C(d, t, r)$ is typically not desirable as it can confuse training and give misleading results. Depending on the application, the required number of needed Tx, Rx, or signals can be smaller than the ones available in the dataset. To reduce the dataset imbalance, the user would typically start by choosing a subset of the dataset.

B. CREATING SUBSETS

To choose a subset, we need to specify a set of N transmitters $\mathcal{T}$ and a set of M receivers $\mathcal{R}$. The choice of a subset determines the minimum number of signals per Tx-Rx pairs K. The variables N, M, and K are dependent; that is we can specify only two variables and the third one is upper bounded by the dataset. To make it easier for WiSig users to choose the transmitter and receiver subsets, we provide a utility which maximizes the number of Rx such that at least a fraction p of N Tx have at least K signals. This problem can be formulated as follows for a given day d

$$\underset{\mathcal{T},\mathcal{R}}{\text{maximize}}\ |\mathcal{R}| \tag{1}$$

$$\text{subject to} \sum_{t\in\mathcal{T}} I\left[C\left(d, t, r\right) \geq K\right] \geq p|\mathcal{T}| \quad \forall\, r \in \mathcal{R} \tag{2}$$

where $I[\cdot]$ is the indicator function which takes a value of one if the constraint is satisfied and $|\cdot|$ denotes the size of the set, thus $|\mathcal{T}| = N$ and $|\mathcal{R}| = M$.

This problem can be formulated as a mixed integer linear programming (MILP). While optimal, the MILP solution can be time consuming. So we developed a simple greedy algorithm which gave satisfactory results when $p = 1$. The MILP formulation is discussed in the appendix. The greedy heuristic works as follows: we start by choosing the Tx having the most Rx that have at least K signals. For these transmitters, we choose the receivers satisfying the constraint (2).

The values of M obtained using the greedy algorithm is shown in Fig. 9a when considering the minimum over all days, that is $C'(t, r) = \min_d C(d, t, r)$ for $p = 1$. Fig. 9a shows that, as expected, number of increasing either the required transmitters N or K yields a smaller number of Rx M. The problem with using $p = 1$ is that even a single Tx-Rx pair not having K signals would eliminate that Rx entirely. To relax this constraint, we can use $p = 0.9$, for example; that is, only 90% of Tx should satisfy the signal requirement per Rx. For $p = 0.9$, we used the MILP formulation because the heuristic did not yield acceptable results. The MILP results are shown in Fig. 9b; note that a larger portion of the dataset can now be utilized.

TABLE 2. Description of compact datasets.

Name	N (Tx)	M (Rx)	K (Sig)	p	Days
ManySig	6	12	**1000**	1.0	4
ManyTx	**150**	18	50	0.9	4
ManyRx	10	**32**	200	0.9	4
SingleDay	28	10	800	1.0	**1**

C. PREPACKAGED COMPACT SUBSETS

To eliminate the need to download the full dataset just to use a subset, we provide conveniently pre-packaged compact subsets. We provide 4 subsets as shown in Table 2. These subsets were designed to cater to different possible use cases. The first subset ManySig was designed to be balanced and provide 1000 signals for all Tx-Rx pairs over all days. ManyTx focuses on increasing the number of transmitters and provides 150 Tx, while tolerating a slight imbalance ($p = 0.9$). ManyRx provides signals captured by a relatively large number of 32 Rx with a slight imbalance. All the previous subsets include data from all 4 days. For users not interested in the impact of days (channel variation), we created the SingleDay subset, which provides a relatively large number of signals and Tx but only for one day. The required download sizes for different versions of the dataset are shown in Table. 3. Note that whereas the raw signal dataset would have required a tremendous 1.4 TB download, the size gets reduced to 76.9 GB after processing, while the pre-packaged subsets are a few GB each, which is more convenient.

VI. USE CASES & OPEN PROBLEMS

The purpose of this section is to demonstrate a few of the possible use cases of WiSig and highlight some of the open problems in transmitter identification. The considered evaluation setup is simple as the results provided are only meant to identify open problems. In this setup, we only consider the problem of closed-set classification among a fixed predetermined set of transmitters using a simple convolutional neural network architecture.

Unless otherwise stated, we used the same neural network consisting of 5 convolutional layers— each followed by max pooling—with three dense layers at the end. The convolutional layers used 8, 16, 32, and 16 filters of sizes (3,2), (3,2),

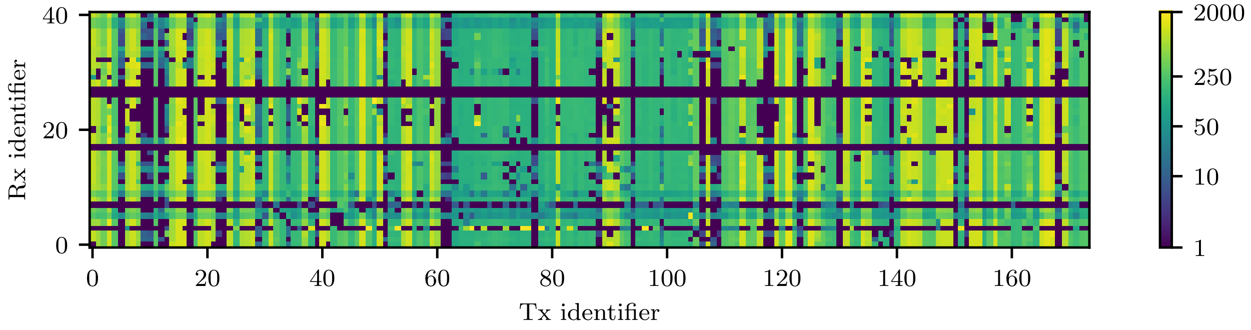

FIGURE 7. The signal count for each Tx-Rx pair on the first day using a logarithmic colormap. Some Rx did not capture any signals for that day. Due to the fact that Rx are not synchronized and possibly due to detection errors, the signal count from different Rx for the same Tx can be significantly different.

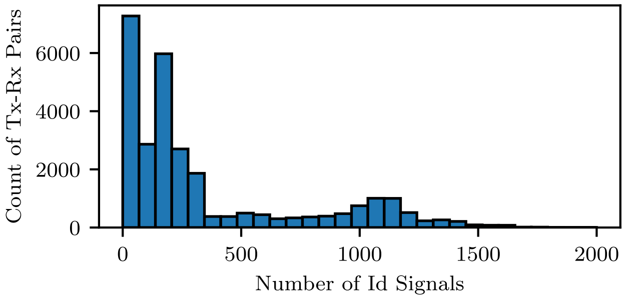

FIGURE 8. Histogram showing the count of Tx-Rx pairs having a given number of signals. The histogram is calculated over all days for the non-equalized Full WiSig.

TABLE 3. WiSig download size.

Name	Signal	Download Size
Raw WiSig	Raw	1.4 TB
Full WiSig	Processed	76.9 GB
WiSig ManySig	Processed	1.4 GB
WiSig ManyTx	Processed	2.5 GB
WiSig ManyRx	Processed	1.2 GB
WiSig SingleDay	Processed	1.0 GB

(3,2),(3,1), and (3,1) respectively. The dense layers used 100, 80, and N units. All layers used ReLU activation except the output layer, which used softmax. The network was trained for 100 epochs with early stopping if the validation loss did not decrease for 5 epochs, and the best weights were retained. The loss function used is categorical cross-entropy defined as $-\sum_{i=0}^{N_c} y_i \log \hat{y}_i$, where N_c is the number of classes, $y_i = 1$ if i is the correct class for the signal and zero otherwise, and $\hat{y}_i$ is the output of the softmax function for that class. Each dataset was divided as 80% for training 10% for validation and 10% for testing. All signals were normalized to have unit average power prior to using them. We now move on to studying the generalization across receivers, days, and the impact of the number of transmitters, and the number of signals on classification. We also show that WiSig can be used for localization.

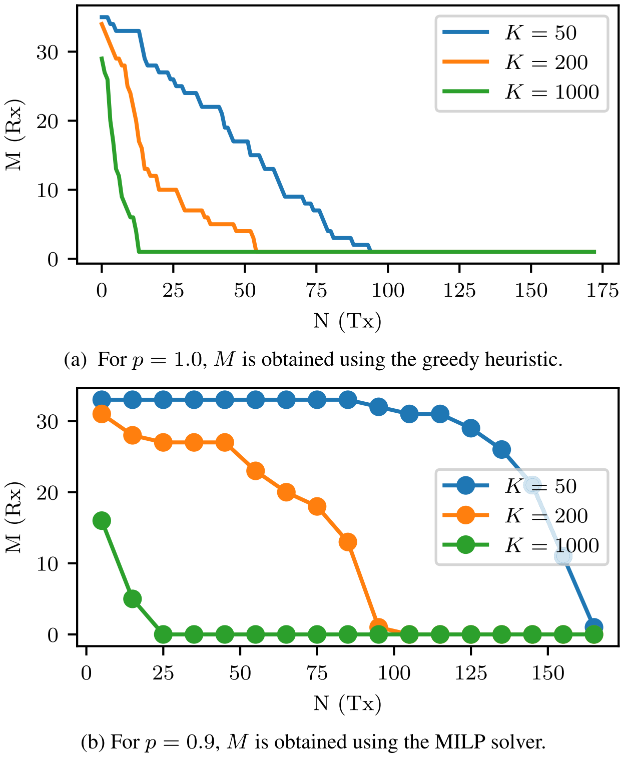

(a) For $p = 1.0$, M is obtained using the greedy heuristic.

(b) For $p = 0.9$, M is obtained using the MILP solver.

FIGURE 9. The number of Rx (M) for a given number of Tx (N) in WiSig, such that at least a fraction p of Tx per Rx has at least K signals. Using $p = 0.9$ utilizes a larger number of Rx than $p = 1$.

A. GENERALIZATION ACROSS RECEIVERS

Many wireless deployments involve multiple access points, and thus require transmitter authorization to be deployed on many receivers. Therefore, it is important to investigate the impact of the receiver fingerprint on classification accuracy. To do that, we use the ManyRx dataset, having 32 receivers. To reduce the impact of channel variation associated with changing the receivers, we used the equalized dataset and just a single day. We randomly chose a subset of these receivers, combined their data captured for the same set of Tx, and used them to train a Tx classifier. The number of receivers in this subset was varied and for each size we trained a classifier. Then, we evaluated each trained classifier using two test sets:

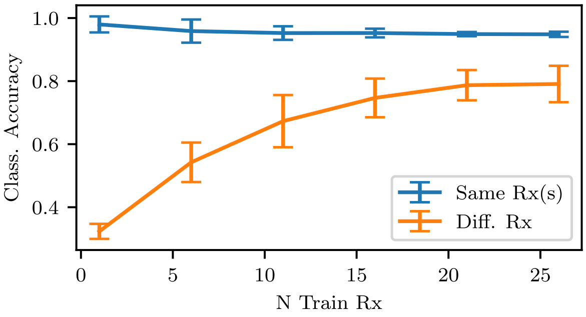

FIGURE 10. The classification accuracy as a function of the number of receivers used in training. A neural network is trained for each number of Rx and is evaluated using data from the same training Rx and then using 5 different Rx. The equalized data is used from the ManyRx subset having 10 Tx.

the first one uses data from the same receivers as those used in training ("Same Rx") and the other one uses 5 entirely different receivers not used during training ("Diff. Rx"). The purpose of this division is to investigate whether a trained classifier can be used on a different receiver than those used to collect the training data. To increase the confidence in the results, we used 5 random realizations of the receiver sets, and show the results as mean and standard deviation in Fig. 10. Looking at the "Same Rx" curve, increasing the number of Rx slightly degrades the accuracy, which is expected, as increasingly more Rx fingerprints need to be learned. However, the average accuracy remains above 95%. When we use different receivers for evaluation, the performance is impacted significantly: for example, using only one Rx for training results in a drop in accuracy from 99% to less than 33%. This huge drop shows that a transmitter classifier trained on one Rx is not expected to work well on another Rx due to the impact of the receiver fingerprint. As we increase the number of training Rx, the testing accuracy on different Rx improves, showing that including captured signals from more Rx during training can improve generalization to new Rx. However, the improvement starts to saturate at about 20 Rx.

While using many Rx in the training capture is simple, it might not always be feasible; a large number of Rx might not be available during training. Ideally, we want to capture the Tx fingerprint using only one Rx and apply it to any Rx. Since the receiver fingerprint is also due to manufacturing variability and is hard to model, data-driven solutions are needed. One solution is to develop Rx fingerprint augmentation techniques. Once trained, such an approach would use signals from one Rx to synthesize signals from other virtual receivers similar to the approach used in [15] for generating open-set classification outliers. Another approach is to develop a technique that can extract receiver independent features. Either one of these approaches could be developed and evaluated using WiSig.

B. GENERALIZATION ACROSS DAYS

Any real-life transmitter authorization deployment is expected to work over a prolonged period of time. As such, we use WiSig to evaluate the performance of a trained transmitter classifier over time. To do that, we use the data from a single receiver from the ManySig dataset for both training and testing; the last day is reserved for testing and the first three days are used for training. We trained several networks using the data from either one, two or all three days and using both the non-equalized and equalized datasets. Then we evaluated them using data from the same days used in training as well as from the different day. The results are shown in Fig. 11. When the evaluation is performed on the same day (both training and testing data collected in the same 0.5s capture), accuracies exceeding 99% are obtained. However, when tested on the different day data (captured a few weeks later) the accuracy drops as previously demonstrated in [1]. As expected, including data from more days during training improves generalization. Equalizing the dataset reduces the channel variability, which decreases the performance degradation on a different day. However, there is still a small drop in accuracy for different days even with equalization, which might be because some aspects of the Tx fingerprint or Rx fingerprint may vary slightly over time [3].

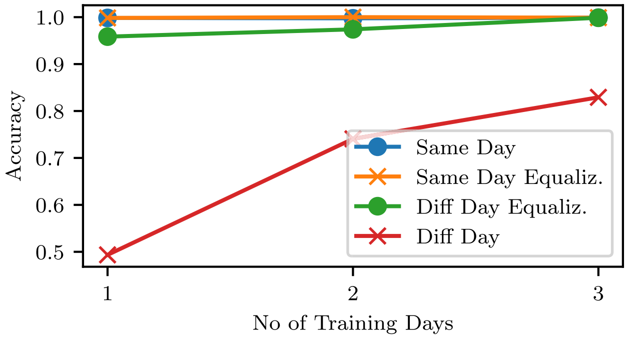

FIGURE 11. The classification accuracy as a function of the number of days used in training for the same Rx. Two neural networks are trained for each number of days: one for the non-equalized and one for the equalized data. Each network is evaluated using data from the same training days and a different day. The ManySig subset, having 6 Tx, is used.

To better understand the difference between signals captured on different days, we compare the channel estimates from two different days. To that end, we consider a single transmitter (node 1-1) and a single receiver (node 20-20). For all the packets from this Tx-Rx pair over two days (March 1st and 8th), after per-packet power normalization, we calculated the magnitude of the channel for all the 52 occupied WiFi subcarriers. In Fig. 12, we plot the mean and standard deviation of the channel calculated over all packets for each day; we can see clearly that the channel differs significantly between the two captures, even though we used the same Tx and Rx. This difference can be explained by changes in the propagation environment (for example people moving objects), which occurred during the week separating the two captures.

Of course, capturing data over a prolonged period of time for robust transmitter identification is not desirable. Ideally, we only want to isolate the Tx fingerprint using just one

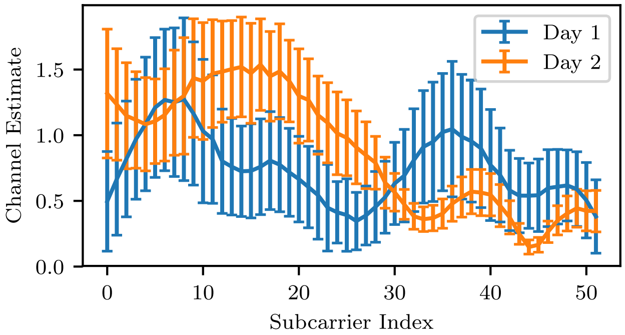

FIGURE 12. The channel estimates of the 52 occupied subcarriers over 2 days. The curve represents the mean of all packets and the error bars represent the standard deviation. The packets were power-normalized.

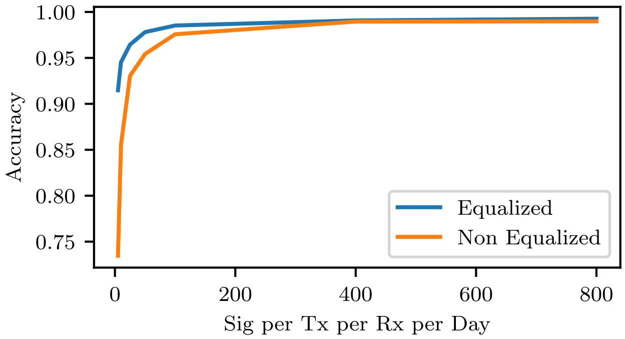

FIGURE 13. The classification accuracy as a function of the number of signals per Tx per Rx and per day. A neural network is trained for each point. Data from all days and receivers in the ManySig subset is used for both training and evaluation.

capture of a short duration. To achieve that goal, we can use channel augmentation techniques, whether handcrafted or data-driven similar to those proposed in [16]. Another approach is to use neural network architectures robust to channel variations similar to [17]. Further investigation is needed to understand how both days and receivers impact performance and whether using additional receivers can compensate for channel variation along days. WiSig provides the data needed for these studies.

C. IMPACT OF NUMBER OF TRAINING SIGNALS

Another aspect to consider is the number of signals needed to train a transmitter identification system and whether we should equalize signals or not. The WiSig dataset can be used to address these questions. Using the ManySig dataset, we train multiple classifiers each using a different number of signals per Tx per Rx per day. We consider all 4 days and all 12 Rx in ManySig and we repeat the experiment with the non-equalized and the equalized datasets. Both the training and test signals are from the same Tx, Rx, days, and state of equalization. The results are shown in Fig. 13. For a small number of signals, equalizing the dataset significantly improves the performance because it reduces the randomness from the channel and makes the task easier. As we increase the number of signals, the accuracy of both approaches improves and the gap between them diminishes. With enough signals from all days and Rx, classifiers can counteract the randomness from the channels.

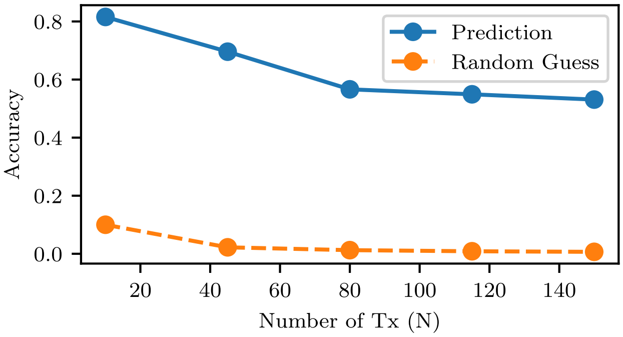

FIGURE 14. The classification accuracy as a function of the number of transmitters *N*. A neural network is trained for each point. Non-equalized data from all days and receivers in ManyTx is used for both training and evaluation. The random guess corresponds to 1/*N*.

Clearly, having more signal improves classification performance. However, that might not always be feasible and neural network architectures that are data-efficient are needed. The minimum number of signals needed for different number of receivers, and days is also still an open problem [18]. Currently, the equalization is implemented using signal processing using the known WiFi preambles. However, a neural network that can blindly equalize the signal for fingerprinting is desirable. Additionally, having a large number of signals can enable researchers to better evaluate the robustness of transmitter fingerprinting against sophisticated adversarial attackers [19]. The WiSig dataset can be used to address these open problems.

D. IMPACT OF NUMBER OF TRANSMITTERS

Depending on the application, a transmitter authorization system might need to authenticate hundreds of users. WiSig enables the evaluation of transmitter authorization at this large scale of users with the ManyTx dataset containing signals from 150 transmitters. To showcase this dataset, we evaluate the impact of the number of transmitters N on classification accuracy. Considering all days and receivers, for each N, we train a classifier and evaluate it on the same non-equalized data. The results are shown in Fig. 14. When using 4 days, 19 Rx, and only 50 signal per Tx per Rx per day, the classification accuracy with just 10 Tx is around 80%. The accuracy is not very high because of the limited number of signals and the challenging structure including many Rx and days. As we increase the number of Tx, the problem becomes more challenging and the accuracy drops to about 53% with 150 Tx. This highlights the need for neural network architectures that can perform well for a large number of transmitters.

Having many transmitters can enable using more practical formulations of the problem. For instance, instead of classifying among a closed set of known transmitters, open set recognition enables rejecting unauthorized transmitters

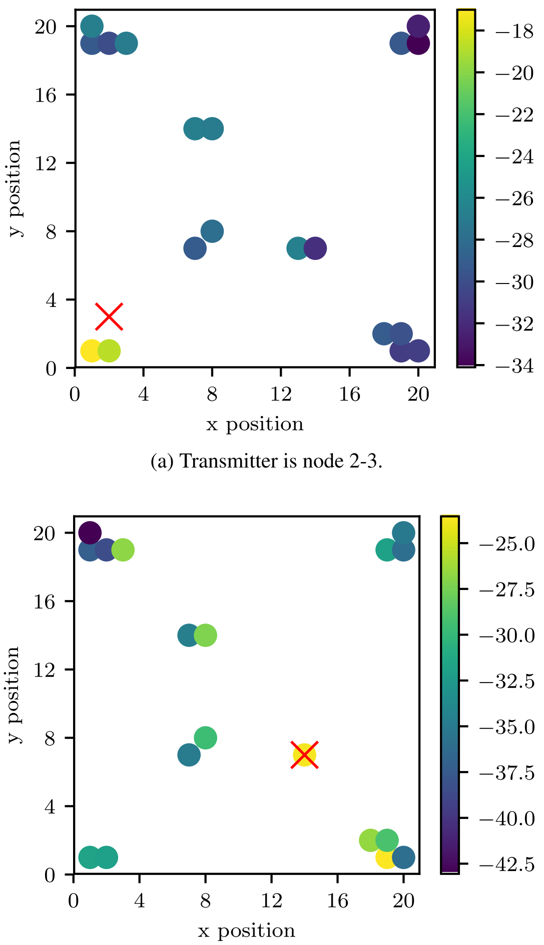

(a) Transmitter is node 2-3.

(b) Transmitter is node 13-7. No data from Rx 14-7.

FIGURE 15. Average baseband received power from two different transmitters as seen by all receivers. Transmitters are shown as red crosses and receivers as circles. The Rx color indicates the average baseband received power in dBm. The ManyTx dataset is used.

unseen in training [12]. The challenge in developing these systems is that different Tx are needed for training and testing, as unauthorized transmitters cannot be exposed during training. Thus a large number of Tx is needed. Furthermore, by encoding the fingerprints to vectors and inserting them into a database, fingerprinting can also become a lookup operation similar to what was proposed in [5], [20]. Thus it is clear that the many transmitters provided by WiSig enable the development of novel architectures and exploring different ways to pose the authorization problem.

E. LOCALIZATION USING MULTIPLE RECEIVERS

Although the WiSig dataset was developed for RF fingerprinting, the grid structure of transmitters and receivers enables using WiSig for localization. To demonstrate that, for each transmitter, we calculated the average baseband power for all its packets as received by different Rx on one day. Using the ManyTx subset, the results are shown in Fig. 15a and 15b for two example transmitters shown as a red cross. The 18 Rx are plotted as circles with the power represented by the heatmap in dBm. As expected, receivers closer to the transmitter have a higher power than those further away. This power received by all Rx creates a location fingerprint, which we removed in the previous results by normalization. To demonstrate that the Rx power can be used for localization, we trained a neural network using the location fingerprint consisting of 18 power measurements. For the missing Tx-Rx pairs, to avoid providing clues to the neural network, a random number within the maximum and minimum receiver power is used instead. The network consisted of three dense layers, consisting of 100, 80, and 2 units respectively. It was trained to predict the x-y coordinate of the transmitter using the mean squared error loss. The trained network provided an L1 error of 1.5 m on the test set. Since the grid separation is 1 m, each transmitter can be confused with its 2 nearest neighbors and only 8% of the 150 Tx were accurately identified on the grid using their locations. While WiSig might not be the best dataset for localization research, it can enable combining localization and Tx fingerprinting. Localization using power can be used to estimate the location of the transmitters and fingerprinting can identify them at much higher accuracy than just relying on localization.

VII. CONCLUSION

In this paper, we presented WiSig as a large-scale dataset for transmitter fingerprinting. A preliminary evaluation using WiSig demonstrated the detrimental impact of changing training days, receivers, and limited training signals on performance. Although including more days, receivers, training signals, or equalizing leads to improved generalization, it might not always be feasible. Novel approaches are needed to develop more robust fingerprinting systems with less strict training data requirements. Further analysis is needed to fully understand the combined effects of training days, and number of receivers, transmitters, along with equalization on performance and to specify the required data collection requirements for good performance. By highlighting some of the open problems and making the data publicly available in an easily accessible manner, we aim to empower future research in transmitter fingerprinting.

APPENDIX

MILP SUBSET CREATION

A more general version of the problem in (1)-(2) was used for the MILP formulation found in the accompanying helper code, and is presented below. $\mathcal{R}$ and $\mathcal{T}$ respectively represent the subsets of chosen transmitters and receivers, while $\mathcal{D}$ represents the set of all days. C_{eq} is the counterpart to C that contains the equalized signals. $\mathcal{R}$ and $\mathcal{T}$ were chosen such that the specified requirements were met across all days and across both the non-equalized and equalized data.

$$\begin{aligned} \underset{\mathcal{T},\mathcal{R},k}{\text{maximize}} \quad & w_{\infty}M + k \\ \text{subject to} \quad & \sum_{t\in\mathcal{T}} I\left[C\left(d,t,r\right) \geq K\right] \geq pN \quad \forall r \in \mathcal{R},\ d \in \mathcal{D} \\ & \sum_{t\in\mathcal{T}} I\left[C_{\text{eq}}\left(d,t,r\right) \geq K\right] \geq pN \end{aligned}$$

$$
\begin{aligned}
&\forall r \in \mathcal{R},\ d \in \mathcal{D}\\
&C\left(d,t,r\right) \geq k \quad \forall r \in \mathcal{R},\ d \in \mathcal{D},\ t \in \mathcal{T}\\
&C_{\text{eq}}\left(d,t,r\right) \geq k \quad \forall r \in \mathcal{R},\ d \in \mathcal{D},\ t \in \mathcal{T}\\
&k \geq K_{\text{low}}\\
&|\mathcal{T}| = N
\end{aligned}
$$

For this implementation, the following requirements were imposed:

- The user specifies $N = |\mathcal{T}|$, K and p as in (1)-(2). In addition, the user is also allowed to specify K_{low}: for any $r \in \mathcal{R}, d \in \mathcal{D}, t \in \mathcal{T}$ where $C(d,t,r) < K$, K_{low} imposes a lower bound by ensuring that $C(d,t,r) \geq K_{\text{low}}$. This essentially allows the user to specify a tolerance level for K. Note that in (1)-(2), $K_{\text{low}} = 0$.
- For $r \in \mathcal{R}, t \in \mathcal{T}$, let $k = \min_{t,r} C_{\min}(t,r)$ where $C_{\min}(t,r) = \min_d \min\left\{C(d,t,r), C_{\text{eq}}(d,t,r)\right\}$. The objective is to find $\mathcal{R}, \mathcal{T}$ that first maximizes $M = |\mathcal{R}|$, and then maximizes k such that $|\mathcal{R}|$ is not reduced. This hierarchical optimization can be achieved by giving an extremely large weight w_∞ to M.

The MILP formulation of the above problem is given below:

$$\max_{\substack{\mathbf{T},\mathbf{R},\mathbf{Y}\\ \mathbf{Z},\mathbf{Q}\\ \mathbf{Q}_{\text{eq}},k}} \ w_\infty \cdot \mathbf{1}^\top \mathbf{R} + k \tag{3}$$

$$
\begin{aligned}
\text{s.t. } & Y(t,r) \leq T(t) \quad \forall r \in \mathbf{R},\quad t \in \mathbf{T} && (4)\\
& Y(t,r) \leq R(r) \quad \forall r \in \mathbf{R},\ t \in \mathbf{T} && (5)\\
& Y(t,r) \geq T(t) + R(r) - 1 \quad \forall r \in \mathbf{R},\ t \in \mathbf{T} && (6)\\
& Z(t,r) \leq Y(t,r) \cdot U \quad \forall r \in \mathbf{R},\ t \in \mathbf{T} && (7)\\
& Z(t,r) \geq 0 \quad \forall r \in \mathbf{R},\ t \in \mathbf{T} && (8)\\
& Z(t,r) \leq k \quad \forall r \in \mathbf{R},\ t \in \mathbf{T} && (9)\\
& Z(t,r) \geq k - [1 - Y(t,r)] \cdot U \quad \forall r \in \mathbf{R},\ t \in \mathbf{T} && (10)\\
& C_{\min}\left(t,r\right) \cdot Y(t,r) \geq Z(t,r) \quad \forall r \in \mathbf{R},\ t \in \mathbf{T} && (11)\\
& Q(d,t,r) \leq Y(t,r) \quad \forall r \in \mathbf{R},\ d \in \mathbf{D},\ t \in \mathbf{T} && (12)\\
& Q(d,t,r) \leq \bar{C}\left(d,t,r\right) \quad \forall r \in \mathbf{R},\ d \in \mathbf{D},\ t \in \mathbf{T} && (13)\\
& Q(d,t,r) \geq Y(t,r) + \bar{C}\left(d,t,r\right) - 1\\
& \qquad\qquad \forall r \in \mathbf{R},\quad d \in \mathbf{D},\ t \in \mathbf{T} && (14)\\
& Q_{\text{eq}}(d,t,r) \leq Y(t,r) \quad \forall r \in \mathbf{R},\ d \in \mathbf{D},\ t \in \mathbf{T} && (15)\\
& Q_{\text{eq}}(d,t,r) \leq \bar{C}_{\text{eq}}\left(d,t,r\right) \quad \forall r \in \mathbf{R},\ d \in \mathbf{D},\ t \in \mathbf{T} && (16)\\
& Q_{\text{eq}}(d,t,r) \geq Y(t,r) + \bar{C}_{\text{eq}}\left(d,t,r\right) - 1\\
& \qquad\qquad \forall r \in \mathbf{R},\ d \in \mathbf{D},\ t \in \mathbf{T} && (17)\\
& \mathbf{1}^\top q(d,r) \geq p \cdot N \cdot R(r) \quad \forall r \in \mathbf{R},\ d \in \mathbf{D} && (18)\\
& \mathbf{1}^\top q_{\text{eq}}(d,r) \geq p \cdot N \cdot R(r) \quad \forall r \in \mathbf{R},\ d \in \mathbf{D} && (19)\\
& k \geq K_{\text{low}} && (20)\\
& \mathbf{1}^\top \mathbf{T} = N && (21)
\end{aligned}
$$

- Let $\mathbb{B} = \{0,1\}$. $\mathbf{T} \in \mathbb{B}^{N_T \times 1}$ and $\mathbf{R} \in \mathbb{B}^{N_R \times 1}$ are binary variables that denote which transmitters and receivers are selected, respectively, where The total number of transmitters is given by $N_T = 174$ and receivers $N_R = 41$.
- (4)-(6) accomplishes $Y(t,r) = T(t)\ \&\ R(r)$ where $\mathbf{Y} \in \mathbb{B}^{174 \times 41}$ is a binary variable.
- (7)-(10) accomplishes $Z(t,r) = \begin{cases} 0 & ; Y(t,r) = 0 \\ k & ; Y(t,r) = 1 \end{cases}$ where $\mathbf{Z} \in \mathbb{Z}^{N_T \times N_R}$ is an integer variable. Note that U is any upper-bound to $C(d,t,r)$ and $C_{\text{eq}}(d,t,r)$.
- $\bar{\mathbf{C}} \in \mathbb{B}^{N_D \times N_T \times N_R}$, $\bar{\mathbf{C}}_{\text{eq}} \in \mathbb{B}^{N_D \times N_T \times N_R}$ are binary constants and $N_D = 4$ is the number of days. $\bar{C}\left(d,t,r\right) = \begin{cases} 0 & ; C(d,t,r) < K \\ 1 & ; C(d,t,r) \geq K \end{cases}$. $\bar{\mathbf{C}}_{\text{eq}}$ is defined similarly.
- $\mathbf{Q} \in \mathbb{B}^{N_D \times N_T \times N_R}$, $\mathbf{Q}_{\text{eq}} \in \mathbb{B}^{N_D \times N_T \times N_R}$ are binary variables.
  $$Q(d,t,r) = \begin{cases} 1 & ; T(t)\ \&\ R(r)\ \&\ I[C(d,t,r) \geq K] \\ 0 & ; \text{otherwise} \end{cases}.$$
  $\mathbf{Q}_{\text{eq}}$ is defined similarly.
- $q(d,r) \in \mathbb{B}^{N_T \times 1}$ is a slice of $\mathbf{Q}$ where $q(d,r) = \{Q(d,t,r) \mid t \in \mathbf{T}\}$. q_{eq} is defined similarly.

REFERENCES

[1] A. Al-Shawabka, F. Restuccia, S. D'Oro, T. Jian, B. Costa Rendon, N. Soltani, J. Dy, S. Ioannidis, K. Chowdhury, and T. Melodia, "Exposing the fingerprint: Dissecting the impact of the wireless channel on radio fingerprinting," in *Proc. IEEE Conf. Comput. Commun. (INFOCOM)*, Jul. 2020, p. 10.

[2] K. Merchant and B. Nousain, "Toward receiver-agnostic RF fingerprint verification," in *Proc. IEEE Globecom Workshops (GC Wkshps)*, Dec. 2019, pp. 1–6.

[3] G. Shen, J. Zhang, A. Marshall, L. Peng, and X. Wang, "Radio frequency fingerprint identification for Lora using deep learning," *IEEE J. Sel. Areas Commun.*, vol. 39, no. 8, pp. 2604–2616, Aug. 2021.

[4] A. Al-Shawabka, P. Pietraski, S. B. Pattar, F. Restuccia, and T. Melodia, "DeepLoRa: Fingerprinting LoRa devices at scale through deep learning and data augmentation," in *Proc. 22nd Int. Symp. Theory, Algorithmic Found., Protocol Design Mobile Netw. Mobile Comput.*, New York, NY, USA, Jul. 2021, pp. 251–260.

[5] G. Shen, J. Zhang, A. Marshall, and J. Cavallaro, "Towards scalable and channel-robust radio frequency fingerprint identification for Lora," 2021, *arXiv:2107.02867*.

[6] J. Yu, A. Hu, G. Li, and L. Peng, "A robust RF fingerprinting approach using multisampling convolutional neural network," *IEEE Internet Things J.*, vol. 6, no. 4, pp. 6786–6799, Aug. 2019.

[7] A. Elmaghbub and B. Hamdaoui, "LoRa device fingerprinting in the wild: Disclosing RF data-driven fingerprint sensitivity to deployment variability," *IEEE Access*, vol. 9, pp. 142893–142909, 2021.

[8] G. Reus-Muns, D. Jaisinghani, K. Sankhe, and K. R. Chowdhury, "Trust in 5G open RANs through machine learning: RF fingerprinting on the POWDER PAWR platform," in *Proc. IEEE Global Commun. Conf. (GLOBECOM)*, Dec. 2020, pp. 1–6.

[9] DARPA. *Radio Frequency Machine Learning Systems*. Accessed: Jan. 10, 2019. [Online]. Available: https://www.darpa.mil/program/radio-frequency-machine-learning-systems

[10] T. Jian, B. C. Rendon, E. Ojuba, N. Soltani, Z. Wang, K. Sankhe, A. Gritsenko, J. Dy, K. Chowdhury, and S. Ioannidis, "Deep learning for RF fingerprinting: A massive experimental study," *IEEE Internet Things Mag.*, vol. 3, no. 1, pp. 50–57, Mar. 2020.

[11] J. Robinson and S. Kuzdeba, "Novel device detection using RF fingerprints," in *Proc. IEEE 11th Annu. Comput. Commun. Workshop Conf. (CCWC)*, Jan. 2021, pp. 0648–0654.

[12] S. Hanna, S. Karunaratne, and D. Cabric, "Open set wireless transmitter authorization: Deep learning approaches and dataset considerations," *IEEE Trans. Cognit. Commun. Netw.*, vol. 7, no. 1, pp. 59–72, Mar. 2021.

[13] D. Raychaudhuri, I. Seskar, M. Ott, S. Ganu, K. Ramachandran, H. Kremo, R. Siracusa, H. Liu, and M. Singh, "Overview of the ORBIT radio grid testbed for evaluation of next-generation wireless network protocols," in *Proc. IEEE Wireless Commun. Netw. Conf.*, vol. 3, Mar. 2005, pp. 1664–1669.

[14] E. Perahia and R. Stacey, *Next Generation Wireless LANs: 802.11N and 802.11AC*. Cambridge, U.K.: Cambridge Univ. Press, May 2013.

[15] S. Karunaratne, S. Hanna, and D. Cabric, "Open set RF fingerprinting using generative outlier augmentation," in *Proc. IEEE Global Commun. Conf. (GLOBECOM)*, Dec. 2021, pp. 1–7.

[16] N. Soltani, K. Sankhe, J. Dy, S. Ioannidis, and K. Chowdhury, "More is better: Data augmentation for channel-resilient RF fingerprinting," *IEEE Commun. Mag.*, vol. 58, no. 10, pp. 66–72, Oct. 2020.

[17] C. N. Brown, E. Mattei, and A. Draganov, "ChaRRNets: Channel robust representation networks for RF fingerprinting," 2021, *arXiv:2105.03568*.

[18] T. Oyedare and J.-M.-J. Park, "Estimating the required training dataset size for transmitter classification using deep learning," in *Proc. IEEE Int. Symp. Dyn. Spectr. Access Netw. (DySPAN)*, Nov. 2019, pp. 1–10.

[19] S. Karunaratne, E. Krijestorac, and D. Cabric, "Penetrating RF fingerprinting-based authentication with a generative adversarial attack," in *Proc. IEEE Int. Conf. Commun. (ICC)*, Jun. 2021, pp. 1–6.

[20] S. Karunaratne, S. Hanna, and D. Cabric, "Real-time wireless transmitter authorization: Adapting to dynamic authorized sets with information retrieval," in *Proc. IEEE Int. Symp. Dyn. Spectr. Access Netw. (DySPAN)*, Dec. 2021, pp. 302–308.

SAMER HANNA (Graduate Student Member, IEEE) received the B.Sc. degree in electrical engineering and the M.Sc. degree in engineering mathematics from Alexandria University, Alexandria, Egypt, in 2013 and 2017, respectively, and the Ph.D. degree from the University of California, Los Angeles, CA, USA, in 2021. His research interests include the applications of machine learning in wireless communications and coordinated communications using unmanned aerial vehicles.

SAMURDHI KARUNARATNE (Graduate Student Member, IEEE) received the B.Sc. degree in computer engineering from the University of Peradeniya, Sri Lanka, in 2019, and the M.S. degree in electrical and computer engineering from the University of California, Los Angeles (UCLA), in 2021. While at UCLA, he was a part of the Cognitive Reconfigurable Embedded Systems Laboratory (CORES). His research interests include optimization algorithms and the applications of machine learning techniques in wireless communications.

DANIJELA CABRIC (Fellow, IEEE) received the M.S. degree in electrical engineering from UCLA, in 2001, and the Ph.D. degree in electrical engineering from UC Berkeley, in 2007. She is currently a Professor in electrical and computer engineering with the University of California, Los Angeles. Her research interests include millimeter-wave communications, distributed communications and sensing for the Internet of Things, and machine learning for wireless networks co-existence and security. She received the Samueli Fellowship, in 2008; the Okawa Foundation Research Grant, in 2009; the Hellman Fellowship, in 2012; the National Science Foundation Faculty Early Career Development (CAREER) Award, in 2012; and the Qualcomm Faculty Award, in 2020 and 2021. She served as an Associate Editor for IEEE Transactions of Cognitive Communications and Networking, IEEE Transactions of Wireless Communications, IEEE Transactions on Mobile Computing, and *IEEE Signal Processing Magazine*. She is an IEEE ComSoc Distinguished Lecturer.